AIAA 99-0755

Numerical Modeling Studies of Wake Vortices: Real Case Simulations

Shaohua Shen, Feng Ding, Jongil Han,
Yuh-Lang Lin, S. Pal Arya
North Carolina State University
Raleigh, North Carolina

Fred H. Proctor
NASA Langley Research Center
Hampton, Virginia

37th AIAA Aerospace Sciences Meeting and Exhibit
January 11-14, 1999 / Reno, NV

NUMERICAL MODELING STUDIES OF WAKE VORTICES: REAL CASE SIMULATIONS

Shaohua Shen*, **Feng Ding**†, **Jongil Han**‡, **Yuh-Lang Lin**§, **S. Pal Arya**¶
Department of Marine, Earth and Atmospheric Sciences
North Carolina State University, Raleigh, NC 27695

Fred H. Proctor‖
NASA Langley Research Center
Flight Dynamics and Control Division
Hampton, VA 23681-2199

Abstract

A three-dimensional large-eddy simulation model, TASS, is used to simulate the behavior of aircraft wake vortices in a real atmosphere. The purpose for this study is to validate the use of TASS for simulating the decay and transport of wake vortices. Three simulations are performed and the results are compared with the observed data from the 1994-1995 Memphis field experiments. The selected cases have an atmospheric environment of weak turbulence and stable stratification. The model simulations are initialized with appropriate meteorological conditions and a post roll-up vortex system. The behavior of wake vortices as they descend within the atmospheric boundary layer and interact with the ground is discussed.

1. Introduction

To increase airport capacity while maintaining or increasing the present aviation safety levels, National Aeronautics and Space Administration (NASA) initiated the Aircraft Vortex Spacing System (AVOSS) project as an essential element of its Terminal Area Productivity (TAP) program to develop a real-time wake vortex forecasting system for Air Traffic Control (ATC)[1,2].

An accurate estimation of the lifetime and transport of the wake vortices trailing behind airplanes is truly crucial in developing the forecasting systems which are responsible for aviation safety and efficiency. A focal problem is to predict the behavior of wake vortices under different atmospheric environments. Results of field experiments as well as numerical simulations indicate that the atmospheric disturbances, such as turbulence, stratification and wind shear have strong influence on the evolution and transport of wake vortices[3-9].

The development of the forecasting system is based on both observed data and numerical simulations. During the past decades, great efforts have been made to understand the demise mechanism of wake vortices and the impact of ambient turbulence, stratification, wind shear and proximity effects on the vortices. These efforts included the laboratory and observed data as well as numerical modeling[9-15]. However, the behavior of wake vortices still remains elusive due to the intricate interaction of the wake vortex pair with its surrounding atmospheric boundary layer. On the other hand, systematic investigation of these processes is hampered by the environmental conditions. The numerical simulations become more practical with increasing computer power because they allow us to study the behavior of wake vortices in a wider range of meteorological conditions than those measured during field experiments which are restricted to a specific location (sometimes with a unique climatology) and relatively short period of time. But numerical models must be validated using these observational data.

In recent years, the large-eddy simulation (LES) models within the meteorological context have been widely used to study the behavior of wake

*Visiting Assistant Professor
†Research Assistant
‡Research Scientist
§Professor
¶Professor
‖Research Scientist, AIAA member

vortices[15-21]. Numerical modeling efforts play a key role in the development of the AVOSS system. The Terminal Area Simulation System (TASS), a numerical large-eddy simulation model developed by Proctor[22,23], has been adapted to accomplish this objective. The model has been successfully used to investigate the effects of atmospheric turbulence, stratification, wind shear and fog on the decay of wake vortices in both two and three dimensional simulations[9,17]. Proctor[9] simulated the behavior of wake vortices measured during the Idaho Falls and Memphis field programs using the TASS model. His results showed that the TASS model was accurate in simulating transport of wake vortices in two dimensions for stable conditions in which there is little or no ambient turbulence. Han et al.[19-20] investigated the Crow instability and the effect of atmospheric turbulence on the vortex decay using three-dimensional TASS model. Their results agree well with other laboratory and field measurements. It is essential that all aspects of the model simulations be compared and validated with observed data although previous studies have shown that the TASS model is quite successful in simulating vortex decay.

Lidar measurements, coupled with the simultaneous recording of the meteorological data from the field measurements conducted at Memphis during December, 1994 and August, 1995 and at Dallas/Ft. Worth (DFW) Airport during 1997-1998, have provided us with the most reliable data base so far. These data sets contain the information on velocity, temperature, circulation and so on, which supply us enough information to carefully make assessment, validation, and improvement of various numerical models.

Ongoing studies with the TASS model are aimed at understanding and quantifying the decay of wake vortices. A determination of whether the simulations can realistically decay vortices is a necessary first step. The model must be validated before its results are used in developing predictor algorithms for an AVOSS system.

The purpose of this paper is to further validate the TASS model. Three dimensional simulations of cases 1252 and 1273 from the 1995 Memphis field experiments are conducted. Presented are TASS results and comparisons with the measurement data from both of the cases.

In this paper, we first briefly describe the TASS model in section 2. We then describe the initialization of the model and the experiments used to initialize the model in section 3. The results from the simulations are presented in section 4 and, finally, our studies are summarized in section 5.

2. The Model Description

2.1 The Numerical Model

The TASS model used in the present study is a three-dimensional, nonlinear, compressible, non-hydrostatic LES model. The TASS equation set in standard tensor notation is as follows[9,22]:

$$\frac{\partial u_i}{\partial t} + \frac{H}{\rho_0}\frac{\partial p}{\partial x_i} = -\frac{\partial u_i u_j}{\partial x_j} + u_i\frac{\partial u_j}{\partial x_j} + g(H-1)\delta_{i3} + \frac{1}{\rho_0}\frac{\partial \tau_{ij}}{\partial x_j} \quad (1)$$

$$H = \left[\frac{\theta}{\theta_0} - \frac{pC_v}{PC_p}\right] \quad (2)$$

$$\frac{\partial p}{\partial t} + \frac{C_p P}{C_v}\frac{\partial u_j}{\partial x_j} = \rho_0 g u_j \delta_{j3} \quad (3)$$

$$\frac{\partial \theta}{\partial t} = -\frac{\partial \theta u_j}{\partial x_j} + \theta\frac{\partial u_j}{\partial x_i} + \frac{1}{\rho_0}\frac{\partial \tau_{\theta j}}{\partial x_j} \quad (4)$$

where u_i is the component of velocity, t is time, θ is potential temperature and θ_0 is the reference potential temperature. p is deviation of pressure from the reference atmospheric pressure P, ρ_0 is the reference air density, C_p and C_v are the specific heats of air at constant pressure and volume, respectively. H represents the ratio of the reference density of environment to the local density. δ_{i3} is the Kronecker delta. g is the earth's gravitational acceleration and τ_{ij} and $\tau_{\theta j}$ are Reynolds stress and heat flux, respectively.

2.2 The Subgrid Turbulence Model

The dependent variables in TASS are treated as averages over the grid volumes which result in subgrid flux terms. The subgrid flux terms τ_{ij} and $\tau_{\theta j}$ are, respectively, approximated by using first-order closure:

$$\tau_{ij} = \rho_0 K_m D_{ij}, \quad (5)$$

$$\tau_{\theta j} = \rho_0 K_H \frac{\partial \theta}{\partial x_j}, \quad (6)$$

where the deformation tensor D_{ij} is defined as

$$D_{ij} = \frac{\partial u_i}{\partial x_j} + \frac{\partial u_j}{\partial x_i} + \frac{2}{3}\frac{\partial u_k}{\partial x_k}\delta_{ij} \quad (7)$$

For subgrid turbulence, TASS currently uses a conventional Smagorinsky model with modifications for stratification and rotation effects:

$$K_m = (c_s\Delta)^2 |D| (1 - \alpha Ri_S - \beta Ri_R)^{0.5} \quad (8)$$

$$K_H = \alpha K_m, \quad (9)$$

$$Ri_S = \frac{N^2}{D^2}, \quad (10)$$

$$N^2 = \frac{g}{\theta}\frac{\partial \theta}{\partial z}. \quad (11)$$

Here K_m and K_H are the subgrid scale eddy diffusivities of momentum and heat, respectively. Ri_S is the Richardson number due to stratification, N is the Brunt-Väisäla frequency, $\Delta=(2\Delta x 2\Delta x 2\Delta x)^{1/3}$ is the filter width, and $c_s = 0.16$ and $\alpha = 3$ are constants, and β is a constant. The rotational Richardson number, Ri_R, represents the rotational effect on turbulence and is analogous to the effect of stratification.

This analogy between the rotation or streamline curvature and buoyancy was first suggested by Bradshaw[24]. An approximate expression for Ri_R applicable to three-dimensional simulations is

$$Ri_R = \frac{\Omega^2}{D^2} + \frac{|\Omega|}{|D|}, \quad (12)$$

where Ω is the magnitude of three-dimensional vorticity[25]. The above formulation does not require cylindrical coordinates or location of vortex axis, so it can be readily applied to fully three-dimensional systems. Equations (8) and (12) indicate that the eddy viscosity K_m can be effectively reduced within the core of vortices when Ri_R or $|\Omega|/|D|$ is large. Since the above formula cannot discriminate between a shear flow and flow with coherent rotation, a discriminator function is applied such that Ri_R=0 when no coherent rotation is present (thus defaulting to the original Smagorinsky model for pure shear flow[25]). Without Eq. (12), the Smagorinsky subgrid closure model overpredicts the vortex decay rate in the vortex core region and causes unrealistic growth of the core size[26].

In the TASS model, a time-splitting integration scheme is used, in which the time integration is broken into small and large time steps. The acoustic term in the momentum and pressure equations are computed over the small time step, while other terms are calculated over the large time step. The space derivatives are approximated by central differences in quadratic conservative form with 4th-order accuracy for advection terms. Arakawa C grid staggered mesh is employed for all variables[27]. There is a choice of different surface boundary conditions by which one can specify the uniform surface temperature, the surface heat flux or the surface energy budget. There is also an option to choose either open or periodical lateral boundary conditions. A detailed description of the model was given by Proctor[9,22].

In our simulations, periodic boundary conditions are imposed in horizontal directions and zero gradient top boundary conditions and no slip bottom conditions are used in the vertical direction. Surface stresses are computed from similarity theory and the surface heat flux is prescribed.

3. Initialization

3.1 Vortex Initialization

A vortex model recently developed by Proctor[28] is used as an initial wake vortex field for three dimensional simulations. This model is empirical as it is based on field observations of several wake vortices measured early in their evolution and represents the post roll-up, wake-vortex velocity field. The model represents observed wake vortex tangential velocity profile much better than previous models, such as Lamb model. Its tangential velocity, V, is represented as

$$V(r) = \frac{\Gamma_\infty}{2\pi r}\left(1 - e^{-10\,(r/B)^{0.75}}\right), \quad (13)$$

where Γ_∞ is the circulation at $r >> r_c$ (r_c is the initial vortex core radius defined as radial distance of peak tangential velocity) and B is the span of the generating aircraft. The values assumed for initial vortex separation and circulation are derived from aircraft weight W, wingspan B, air density ρ, and airspeed V_a, according to the conventional assump-

tion of elliptically-loaded wing, i.e.,

$$b_0 = \frac{\pi B}{4} \quad \text{and} \quad \Gamma_0 = \frac{4W}{\pi B \rho V_a}. \tag{14}$$

Note that the velocity field in *Eq.*(13) depends on the wingspan B instead of the core radius r_c which may not be easy to measure with a good accuracy; *Eq.*(13) is applied only at $r > r_c$. For $r < r_c$, the model is matched with the Lamb model, i.e.,

$$V(r) = \frac{\Gamma_\infty}{2\pi r} 1.4 \left(1 - e^{-10\,(r_c/B)^{0.75}}\right) \times \left(1 - e^{-1.2527\,(r/r_c)^2}\right). \tag{15}$$

The results from Han et al.[26] show that this initialization procedure gives a good comparison with observation data even though it does not depend on the individual aircraft configuration.

3.2 Measurement Data

The data we used in our simulations come from the experiment conducted at the Memphis International Airport during August, 1995. The purpose of the field experiment was to measure wake vortex, meteorological and aircraft data together at an operational airport for use in validation of wake vortex models and in the development of the AVOSS prediction system. The wake vortex measurements were performed by a van-mounted 10.6 μm CO_2 CW lidar[29]. The lidar measured line-of-sight velocities in a plane perpendicular to the flight path in order to characterize vortices generated by approaching aircraft.

The atmospheric data sets were measured by several instruments, which included a 45m tower instrumented with various meteorological sensors for wind velocity, temperature and humidity, a radar profiler and acoustic sodar for measuring winds aloft, a Radio acoustic sounding system (RASS) for measuring temperature data, and the radiosonde balloon launches for the measurement of vertical profiles of wind speed and temperature[30]. The standard atmospheric variables and the atmospheric fluxes were measured at 1 Hz and 10 Hz, respectively.

In the Memphis field experiment, most of the turbulence data come from the tower measurements at 5 and 40m, the turbulence kinetic energy (TKE) and the energy dissipation rate, ϵ, are only available at heights of 5 and 40m (ϵ was calculated by estimating the spectral energy density). Here, the turbulence intensity is defined as weak, mild or strong in terms of the TKE or ϵ at a height of 40m[31]. From these data sets, cases 1252 and 1273 were chosen for the validation of the TASS model. Both cases have a stable stratification with weak wind shear. The values of wind shear and stratification at the surface and initial vortex height for both cases are given in Table 1.

Flight No.	M-1252	M-1273
$(\partial V/\partial z)_s$	9.3×10^{-2}	1.56×10^{-1}
$(\partial V/\partial z)_h$	4.0×10^{-3}	-3.0×10^{-3}
N^*_s	4.1×10^{-2}	1.12×10^{-1}
N^*_h	-6.8×10^{-4}	2.50×10^{-3}

Table 1. Values of wind shear and stratification for Memphis cases 1252 and 1273

In Table 1, subscript "s" and "h" represent the values at the surface ($z = 3m$) and the initial vortex height, respectively. The vertical shear of crosswind, $\partial V/\partial z$, changes with height, and the nondimensional Brunt-Väisäla frequency is $N^*=2\pi {b_0}^2/\Gamma_0$, where Γ_0 is the initial circulation of the vortices.

The values of the vortex parameters and flight data of the generating aircraft were obtained from the Memphis data set[29]. The flight type, initial circulation, vortex core radius, vortex separation, initial vortex height and sink rate of vortex are shown in Table 2.

Flight No.	M-1252	M-1273
Aircraft	B-757	DC-10
Γ_0 (m^2/s)	345	489
r_c(m)	1.5	2.5
b_0(m)	29.8	39.6
h_0(m)	175.0	169.5
V_0(m/s)	1.87	1.97
b_0/V_0(s)	16.1	20.1

Table 2. Aircraft type and vortex parameters

3.3 Grid/Domain Configuration

The TASS model with the three-dimensional option is chosen to perform all simulations in this paper. The model domains, along the axial, lateral and vertical directions, are $75 \times 150.75 \times 237m$ and $104 \times 202 \times 200m$ for the cases 1252 and 1273, re-

spectively. As shown in Table 2, the initial separation distance of the vortex pair, b_0, is 29.8m in case 1252 and 39.6m in case 1273. The domain size in the axial direction is about $2.5b_0$ for cases 1252 and 1273. Such a small domain size in the axial direction may suppress the development of Crow instability of which theoretical maximum wavelength is about $8.6b_0$ [10] and cause homogeneous vortex decay along this direction in a statistical sense, but it can save much computing time without destroying the main vortex decay mechanism[15] . The domain sizes in lateral directions are approximately $5b_0$ for both cases. The domain sizes in lateral and vertical directions are reasonable for a vortex pair separation of b_0, because the strain rate of neighboring periodic vorices is only a few percent of that exerted by one vortex on the other in the vortex pair.

To save computing time, the TASS model with two meshes of different grid resolution is used to perform our simulations. We first ran the TASS model with a coarse mesh to generate a steady state turbulence. Then all variables are interpolated to fine mesh to simulate the vortex decay. Both coarse and fine meshes cover the same domain. A detailed description of this procedure will be given in the next subsection.

The grid points are, respectively, $50 \times 102 \times 136$ in the coarse mesh and $50 \times 201 \times 316$ in the fine mesh, with grid size $(\Delta x,\ \Delta y,\ \Delta z) = (1.5\,m, 1.5\,m, 1.5\,m)$, and $(\Delta x,\ \Delta y,\ \Delta z) = (1.5m,\ 0.75m,\ 0.75m)$ for case 1252. In case 1273, the grid points are $52 \times 100 \times 100$ and grid sizes are $(\Delta x,\ \Delta y,\ \Delta z) = (2m,\ 2m,\ 2m)$ in the coarse mesh, while the grid points are $52 \times 202 \times 200$ with grid sizes $(\Delta x,\ \Delta y,\ \Delta z) = (2m,\ 1m,\ 1m)$ in the fine mesh. The x, y and z correspond to the axial, lateral and vertical directions of the vortex system and corresponding velocity components of u, v and w, respectively.

3.4 Turbulence Initialization

To simulate the behaviour of wake vortices in a real atmosphere, it is of crucial importance to get an initial field which is analogous to real atmospheric environments. One of the major difficulties in initializing the model for real cases is obtaining a representative ambient turbulence field. The difficulty arises from the intricate interaction of the atmospheric turbulence, stratification and wind shear. In case 1252 and 1273, the turbulence is weak due to stable stratification, especially for case 1252. It is difficult for the model to generate or maintain the observed initial turbulence field under stable stratification conditions without an external forcing because the computational domain in the model does not cover the whole atmospheric boundary layer and there is no energy source to maintain the turbulence.

In our simulations, we first generated a turbulence field in coarse mesh through the surface heating. After turbulence reaches a steady state, we then interpolated the values of all variables in the coarse mesh to the fine mesh. At that time, the wind and temperature profiles deviated from their initial values beause of the surface heating and mixing turbulence. To maintain the initial wind and temperature profiles, we continued to run the model and forced the mean wind and temperature profiles back to their initial values at each time step through the surface cooling. During this period, we monitor the decrease in turbulence kinetic energy (TKE) with time at a height near 40m. The wake vortex pair was injected into the simulation when the TKE at this height was approximately equal to the observed TKE measured at 40m

In this paper, three simulations were performed using the three dimensional TASS model and the cases 1252 and 1273 in the Memphis field measurements were used to validate the model. The first two simulations were designed to further simulate the vortex decay in case 1273 and 1252, respectively. The third simulation was designed to examine the simulation of case 1252.

The vertical profiles of measured temperature and wind velocity that represent the air mass surrounding the wake vortices were used to initialize the simulations (Figs. 1 and 2). We assumed that the ambient temperature and wind velocity are homogeneous in horizontal directions and the ambient velocity along the axial direction of wake vortex (u component)is zero.

The energy dissipation rates and turbulence intensities of the measurements and the three simulations for both case 1252 and 1273 are given in Table 3.

Here $\eta=(\epsilon b_0)^{1/3}/V_0$ and $V_0=\Gamma/2\pi b_0$. "ob" and "sm" represent the values from the observation and simulation, respectively. A second simulation for case 1252 (referred as M-1252-II) is a re-simulation of the first simulation, but with somewhat larger tur-

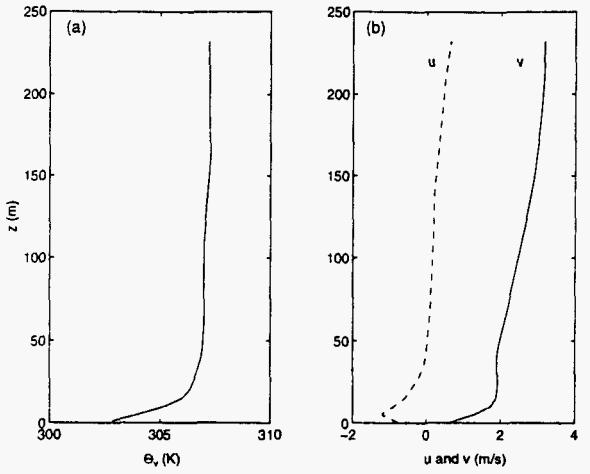

Figure 1. The vertical profiles of (a) virtual potential temperature and (b) wind velocities for case 1252. u (dashed line) and v (solid line) are wind velocity in axial and lateral (crosswind) directions, respectively.

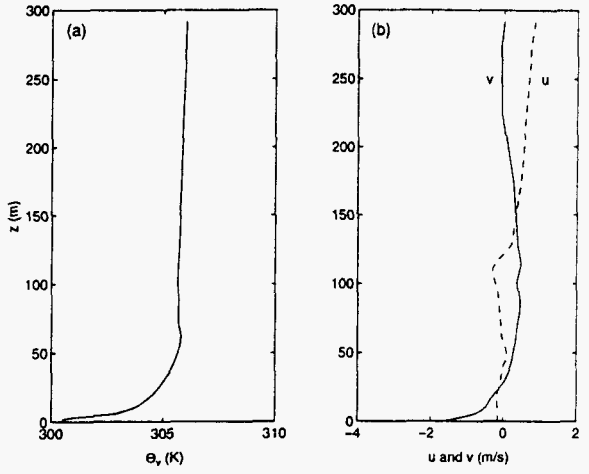

Figure 2. Same as Fig. 1, but for case 1273.

flight No.	M-1273	M-1252	M-1252-II
ϵ(ob)	3.18×10^{-4}	1.35×10^{-6}	1.35×10^{-6}
ϵ (sm)	2.95×10^{-4}	6.27×10^{-6}	4.30×10^{-5}
η (ob)	1.21×10^{-1}	1.84×10^{-2}	1.84×10^{-2}
η (sm)	1.42×10^{-1}	3.05×10^{-2}	5.85×10^{-2}

Table 3. Turbulence intensity

bulence intensity than was observed.

4. Results and Discussion

4.1 Case 1273

In case 1273 a wake vortex is generated by a DC-10 at an elevation of 170 m. The vortices descend through weak crosswind and low turbulence and are not influenced by the ground until after 60 s. The atmospheric temperature profile is weakly stable above 50 m elevation, but becomes increasing stable toward the ground. Results from this case are shown in Fig. 3-6.

Figure 3 shows the radial distribution of normalized circulation for 3-D simulation and Lidar measurement data for case 1273 at t= 15, 45 and 75 second. Comparison of the profiles shows that the circulation computed from the model agrees generally with that measured by the Lidar. Both the simulations and observations show that the circulation decreases with time and the core radius remains a constant.

The circulation decays more or less uniformly with radius as shown in Fig. 3. At t=75s, the vortex has descended to about 35m above the ground (see Fig. 6), where the stratification becomes more stable and the ground begins to interact strongly with the vortex pair.

Figure 3 also indicates that the modeled circulation, in some degree, deviates from the observed circulation. One of the reasons is that the modeled circulation was obtained directly by integrating the vorticity field and then averaging the circulations at all cross-sections along axial direction, while the measured circulation was estimated from Lidar line-of-sight velocities at one cross-section.

The radial distribution of tangential velocity from the simulation and Lidar measurement at t=15, 45 and 75s is shown in Figure 4. It is clear that the tangential velocity decays with increasing time and radial distance. At t=75s, the tangential velocity near the edge of the core radius is reduced to about 30% of its initial value. The rapid decay is caused by the ambient turbulence and stratification, rather than by molecular diffusion and core expansion which need more than several hours to undergo a similar decay. In fact, Fig. 4c shows that the core radius only increase to 3.0m from its initial value of 2.5m. These results agree well with the estimates of Sarpkaya[31].

The averaged circulations of 3-10m and 5-15m are plotted in Figure 5. The 3-10m averaged circulation is well matched with measurements, except for the time less than 10s when the observed circulation was larger than the modeled circulation. In our simula-

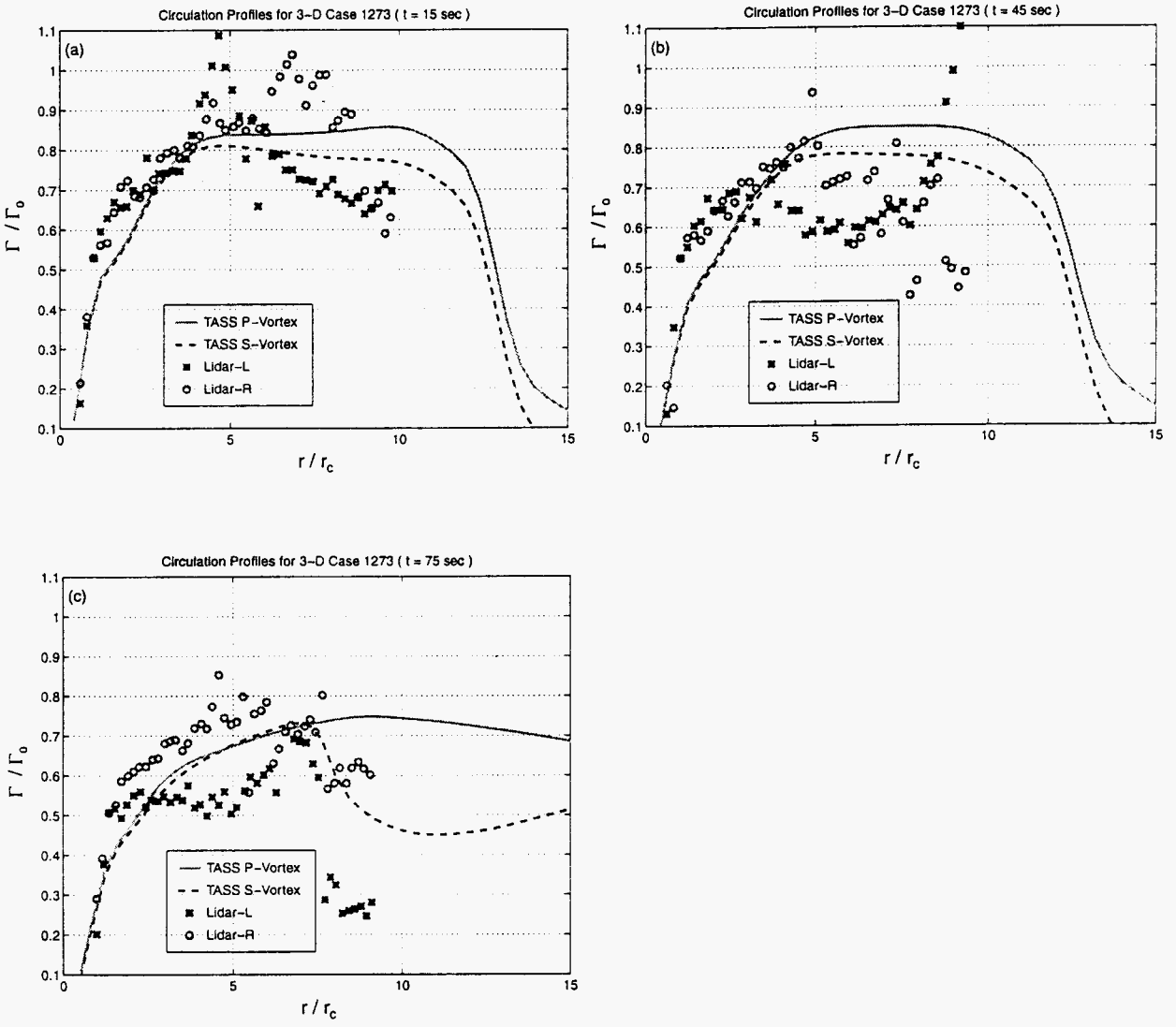

Figure 3. The radial distribution of circulation from the TASS simulation and Lidar measurements for case 1273 at (a) t=15s, (b) 45s and (c) 75s. Circulation is normalized by the initial theoretical circulation, and radius is normalized by the initial core radius (rc=2.5 m). Symbols represent Lidar measurements of left and right sides of port vortex. Solid and dashed lines represent the simulated Port and Starboard vortices, respectively.

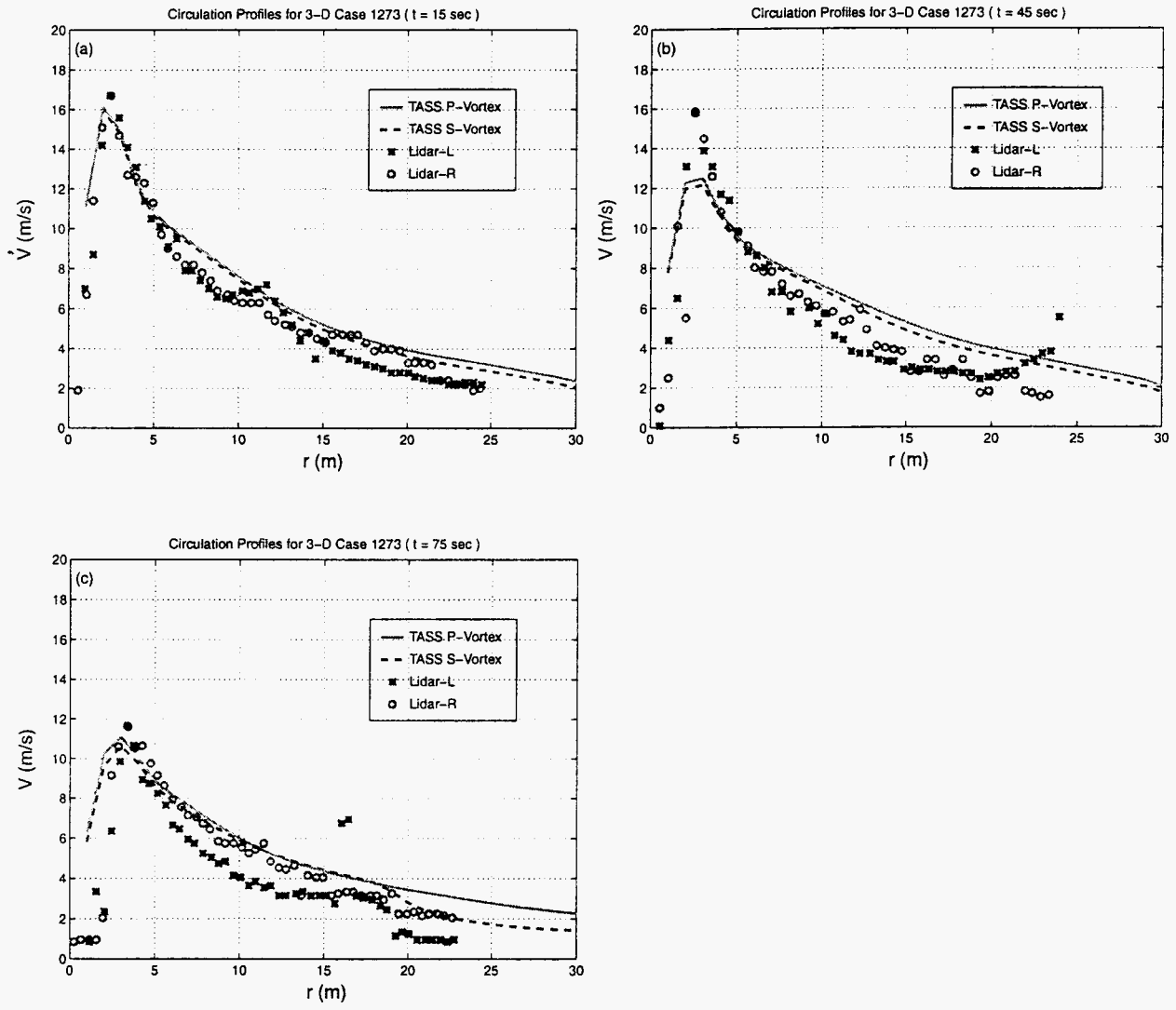

Figure 4. The radial distribution of tangential velocity from the TASS simulation and Lidar measurement for case 1273 at (a) t=15s, (b) 45s and (c) 75s. Symbols represent Lidar measurements of left and right sides of port vortex. Solid and dashed lines represent the simulated port and starboard vortices, respectively.

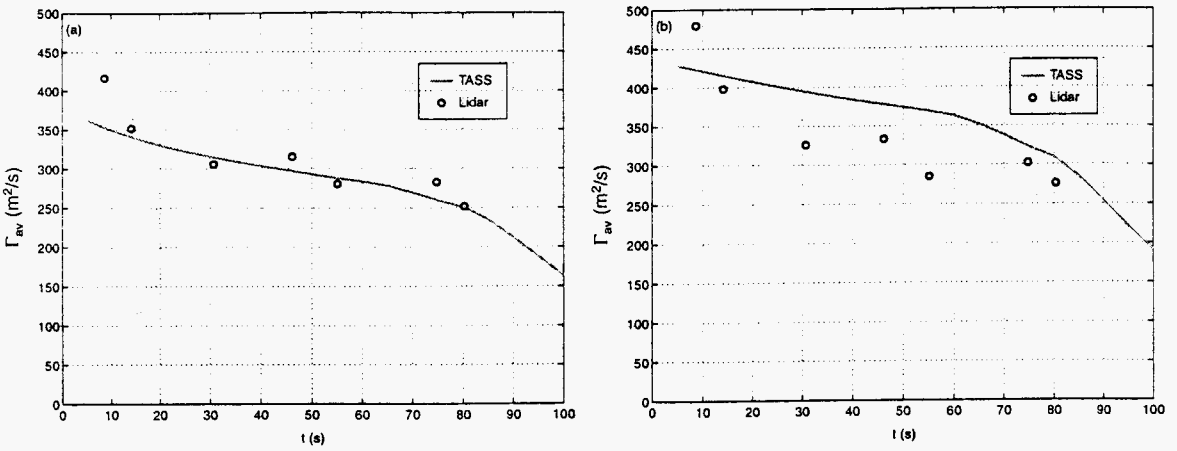

Figure 5. The 3-10m and 5-15m average circulations versus time from both the simulation and measurements for case 1273. (a) the 3-10m average circulation; (b) the 5-15m average circulation.

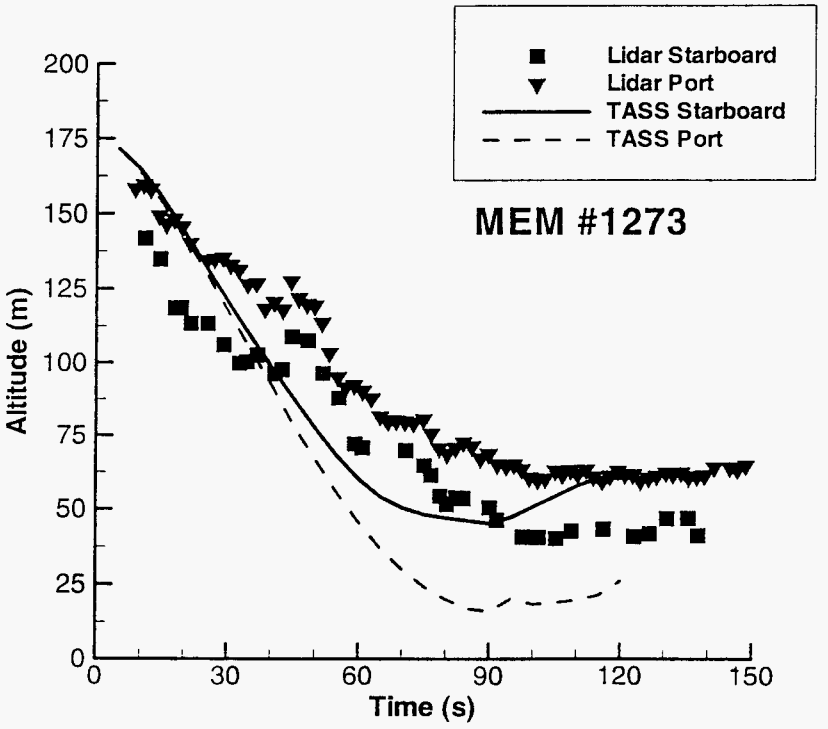

Figure 6. The vortex height history from the simulation and field measurements for case 1273. Symbols represent Lidar measurements. Solid and dashed lines represent the simulated port and starboard vortices, respectively.

tion, the 5-10m averaged circulation decays slowly before t=60s and more rapidly after that time (Fig. 5b). Although the modeled circulations are slightly larger than the observed circulation, the differences are within 20%. The discrepancy at early times may be caused by measurement error, since Campbell et al.[32] have found that the measured Lidar circulations were overestimated during initial times.

Comparisons of the modeled results with field measurements of the vortex trajectories are shown in Figure 6. It can be seen that the development of the vortex height with time from both the simulation and observation is in reasonably good agreement. The vortices linearly descend until at t=60s when they stall due to the stable stratification, windshear, and ground effect. The vortices descended to an average height of 55m at about t=85s. After that time, they rise slightly.

As shown in Fig. 6, the port vortex is deflected to a higher altitude than its starboard counterpart, and the mutual induction between the two vortices is weakened because of the increasing separation between the two vortices. Our simulation is consistent with Proctor's two-dimensional simulation[17], regarding the influence of crosswind shear on vortex descent. Compared with the measurement data (Fig. 6), the starboard vortex descended a lower altitude (about 25m) than that observed (about 40m) during later time of the experiment.

4.2 Case 1252

Case 1252 is somewhat similar to 1273 except that the wake is generated by a B-757 in an environment of slightly weaker stratification and turbulence. Both the simulated and observed wakes descend to the top of the stable layer at 40m in about 100s.

The radial distribution of normalized circulation and tangential velocity from the 3-D simulation and Lidar measurement data for case 1252 at t= 15, 30 and 80s are shown in Figures 7-8. The modeled circulation decays slower than the measured circulation, particularly at t<40s or r/rc > 5. The tangential velocity is well matched with the observation data, except near the core radius where the model under predicts the tangential velocity.

Figure 9 shows the averaged circulations of 3-10m and 5-15m at different times. The model predicts the decay of the 3-10m averaged circulation very well, but under predicts the decay of the 5-15m averaged circulation. Measurement shows decay more rapidly before t=40s. One possible reason for the under prediction of the decay could be an underestimation in the intensity of the ambient turbulence. Therefore, an additional simulation has been run using a slightly higher value of turbulence and will be presented later in this section.

The vortex trajectories from the simulation and observation are shown in Figure 10, and it can be seen that the vortex trajectories are well predicted. Unlike in case 1273, the vortices do not show any rising motion prior to ground interaction. Fig. 10a shows the wake vortices linearly descending with a velocity of 1.8m/s before 70s, but slowly descending after 70s apparently due to the strong stratification and ground effects. The effect of the crosswind is clear in Fig. 10b. Both vortices are transported in the same direction. They move away from the position of generation before 45s and turn back to their original position during later time. This is partly due to the downward transport of crossflow momentum from their generation point. It is worthy to note that the effect of the crosswind is not simple advection since the slope of the lateral position vs time relation is different for both vortices.

To investigate whether the relatively faster decay from the Lidar measurements might have been associated with an under-reported level of turbulence intensity, we have rerun case 1252 with a slightly larger value for ambient turbulence. Otherwise, all conditions are identical with those in the previous simulation, with ϵ now set to $4.3\times10^{-5}m^2/s^3$.

The radial distribution of normalized circulation and tangential velocity for the simulation and Lidar measurement data at t= 30 are shown in Figure 12. It can be seen that the modeled circulation and tangential velocity are well matched with the Lidar measurements. Comparing with Figs. 8-9, the circulation decay is much faster at all radii for the larger intensity of ambient turbulence.

Figure 12 shows that the averaged circulations of both 3-10m and 5-10m are well predicted except that the model slightly over-predicts the decay of the 3-10m averaged circulation after t=60s due to slightly stronger turbulence. Compared with Fig. 9, we can see from Fig. 12 that this simulation better reproduced the behavior of wake vortices. The vortices decay rapidly for the time less than 40s and decay slowly after that time. A possible explanation for

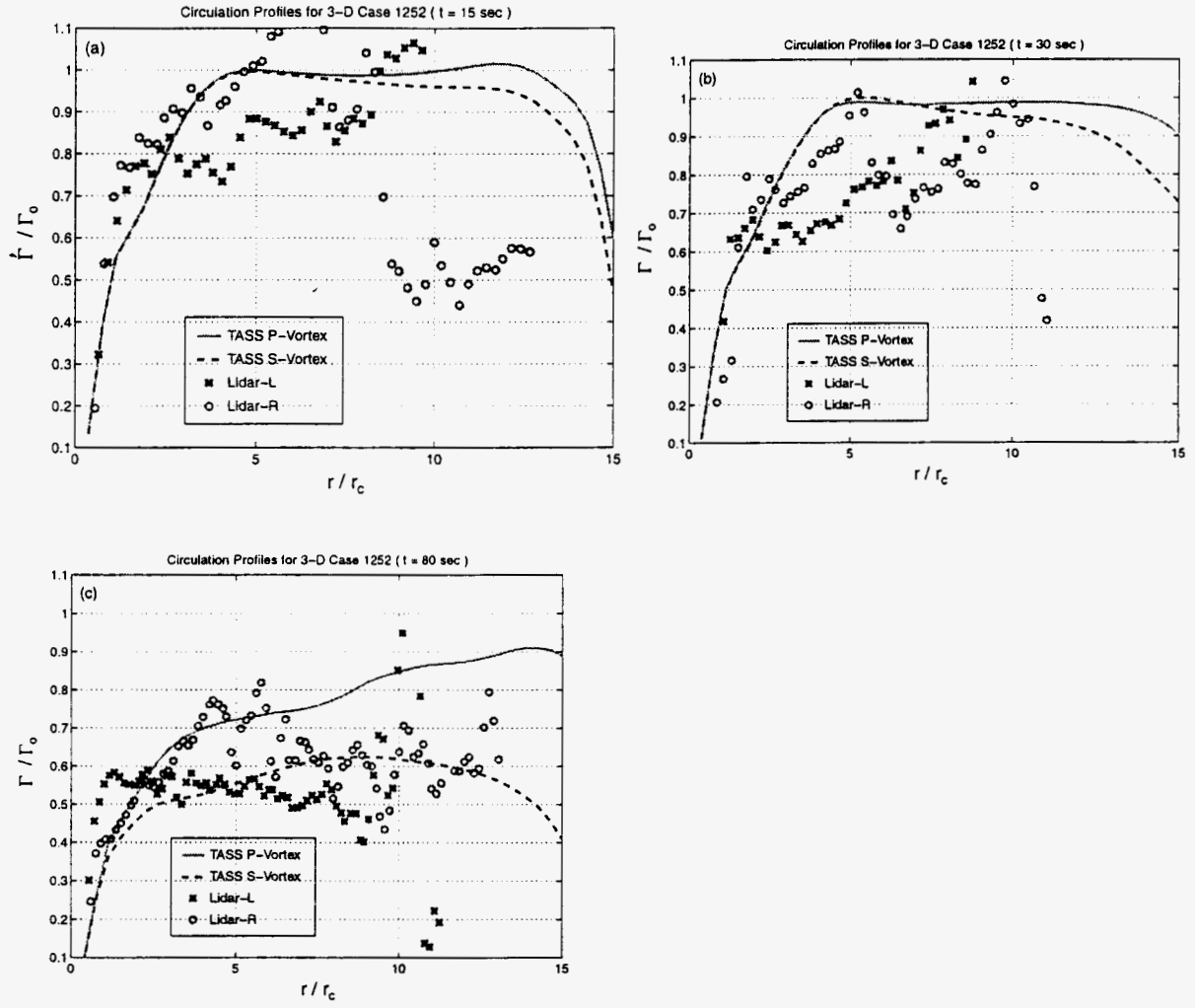

Figure 7. The radial distribution of circulation from the TASS simulation and Lidar measurements for case 1252 at (a) t=15s, (b) 30s and (c) 80s. Circulation is normalized by the initial theoretical circulation, and radius is normalized by initial core radius (rc=1.5 m). Symbols represent Lidar measurements of left and right sides of port vortex. Solid and dashed lines represent the simulated port and starboard vortices, respectively.

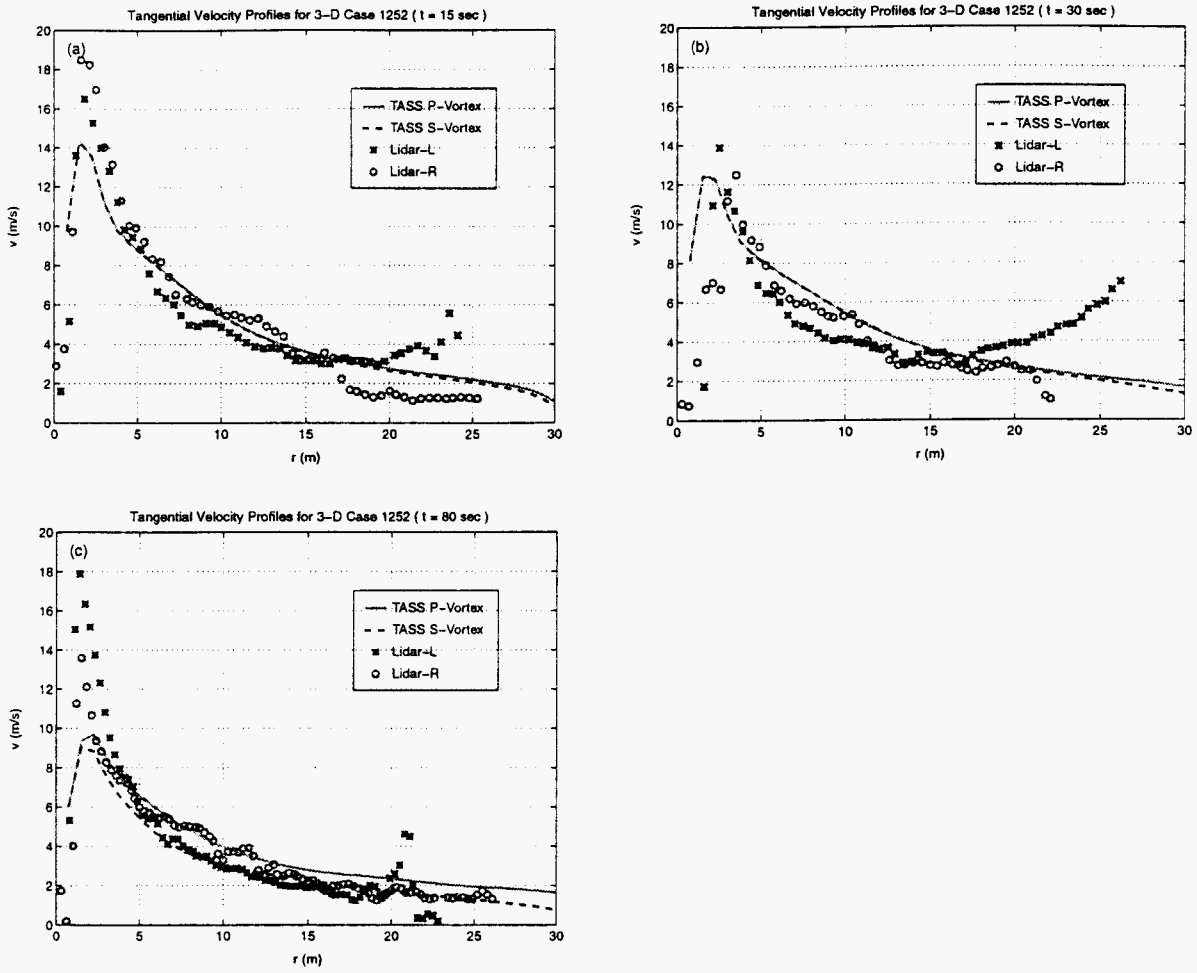

Figure 8. The radial distribution of tangential velocity from the TASS simulation and Lidar measurements for case 1252 at (a) t=15s, (b) 30s and (c) 80s. Symbols represent Lidar measurements of left and right sides of port vortex. Solid and dashed lines represent the simulated port and starboard vortices, respectively.

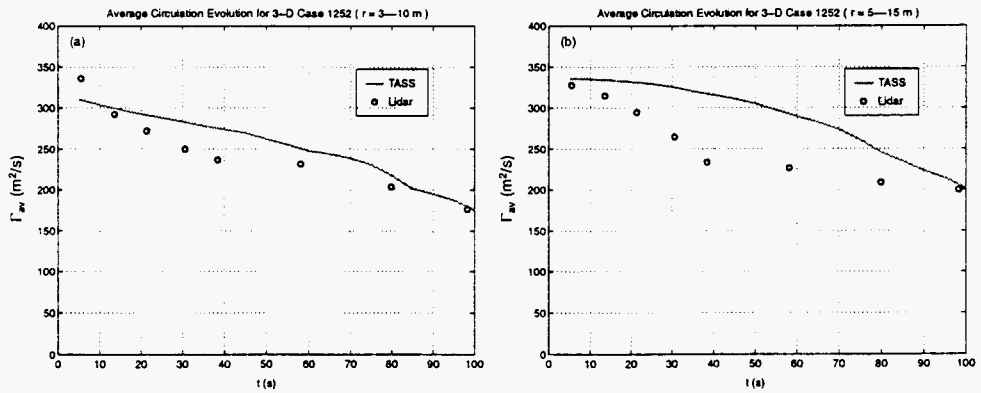

Figure 9. The 3-10m and 5-15m average circulations versus time from both the simulation and measurements for case 1252. (a) the 3-10m average circulation; (b) the 5-15m average circulation.

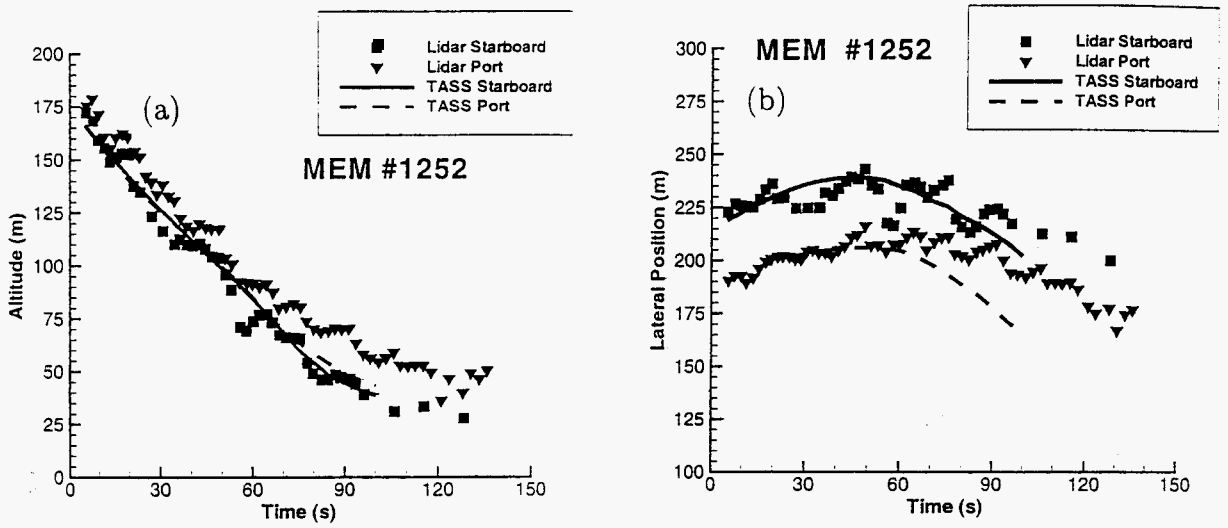

Figure 10. The vortex trajectories from the simulation and Lidar measurements for case 1252. (a) vortex height history; (b)vortex lateral position. Symbols represent Lidar measurements. Solid and dashed lines represent the simulated port and starboard vortices, respectively.

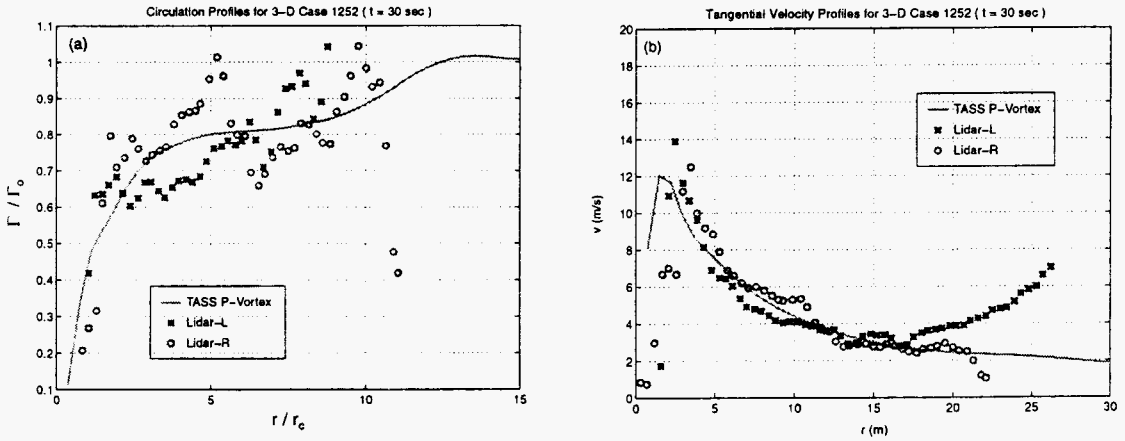

Figure 11. The radial distribution of (a) circulation and (b) tangential velocity from the TASS simulation and Lidar measurements at t= 30s. Circulation is normalized by the initial theoretical circulation, and r_c is initial core radius. Symbols represent Lidar measurements of left and right sides of port vortex. Solid line represents the simulated port vortex.

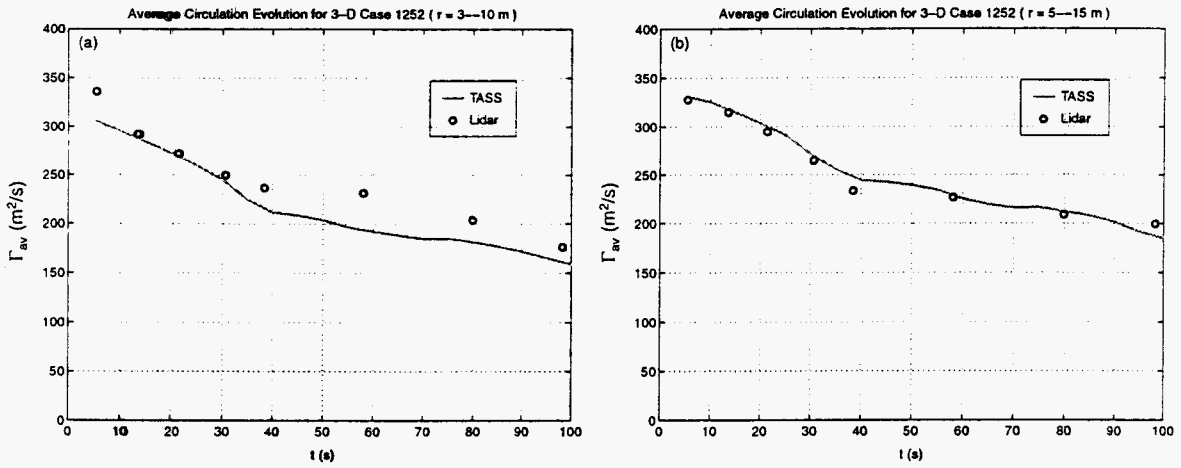

Figure 12. The 3-10m and 5-10m average circulations versus time from the simulation and Lidar measurements. (a) the 3-10m average circulation; (b) the 5-10m circulation.

this good agreement is that the measured dissipation rate was under-estimated or that the value observed at 40 m did not characterize the turbulence intensity at other altitudes.

5. Summary

To validate the application of LES to wake vortex decay, three-dimensional simulations in a realistic atmospheric boundary layer were performed using NASA's TASS model. Two case studies were presented which were initialized from and compared with Memphis fields measurements.

Our results indicate that the TASS model successfully predicted the behavior of aircraft wake vortices within environments representing a transitioning atmospheric boundary layer following sunset. Good agreement was obtained between simulations and measurements for the wake vortex trajectories. Exceptional agreement with the measurements was obtained for vortex decay. The three-dimensional simulations suggest that ambient turbulence, stratification and wind shear play important roles in the decay and transport of wake vortices. Ambient turbulence significantly influences the vortex decay. Study on the specific roles of wind shear, stratification and turbulence on vortex behavior pertinent to these two cases are in progress.

Acknowledgments:

This investigation was supported by NASA Langley Research Center under Cooperative Agreement NCC-1-188. Numerical simulations were performed on NASA's Cray C90 and North Carolina Supercomputing Center's Cray T90. Processed circulation and tangential velocity data for Memphis cases 1252 and 1273 were provided by T. Sarpkaya.

References

[1] Hinton, D. A., "Aircraft Vortex Spacing System (AVOSS) Conceptual Design," *NASA TM-110184*, August 1995.

[2] Perry, R. B., Hinton, D. A., and Stuever, R. A., "NASA Wake Vortex Research for Aircraft Spacing," *35th Aerospace Sciences Meeting & Exhibit*, Reno, NV, AIAA Paper No. 97-0057, January 1997.

[3] Tombach, I., "Observations of Atmospheric Effects on Vortex Wake Behavior," *Journal of Aircraft*, Vol. 10, 1973, pp. 641-647.

[4] Hecht, A. M., Bilanin, A. J., and Hirsh, J. E., "Turbulent Trailing Vortices in Stratified Fluids," *AIAA Journal*, Vol. 19, 1981, pp. 691-698.

[5] Sarpkaya, T., "Trailing Vortices in Homogeneous and Density-Stratified Media," *Journal of Fluid Mechanics*, Vol. 136, 1983, pp. 85-109.

[6] Sarpkaya, T. and Daly, J. J., "Effect of Ambient Turbulence on Trailing Vortices," *Journal of Aircraft*, Vol. 24, 1987, pp. 399-404.

[7] Liu, H. -T., "Effects of Ambient Turbulence on the Decay of a Trailing Vortex Wake," *Journal of Aircraft*, Vol. 29, 1992, pp. 255-263.

[8] Robins, R. E. and Delisi, D. P., "Numerical Study of Vertical Shear and Stratification Effects on the Evolution of a Vortex Pair,"

[9] Proctor, F. H., "Numerical Simulation of Wake Vortices Measured During the Idaho Fall and Memphis Field Programs," *14th AIAA Applied Aerodynamics Conference*, Proceedings, Part-2, New Orleans, LA, AIAA Paper No. 96-2496, June 1996. pp. 943-960. *AIAA Journal*, Vol. 28, 1990, pp. 661-669.

[10] Crow, S. C., "Stability Theory for a Pair of Trailing Vortices," *AIAA Journal*, Vol. 8, 1970, pp. 2172-2179.

[11] Crow, S. C. and Bate, E. R., "Lifespan of Trailing Vortices on a Turbulent Atmosphere," *Journal of Aircraft*, Vol. 7, 1976, pp. 476-482.

[12] Sarpkaya, T. and Daly, J. J., "Effect of Ambient Turbulence on Trailing Vortices," *Journal of Aircraft*, Vol. 24, 1987, pp. 399-404.

[13] Greene, G. C., "An Approximate Model of Vortex Decay in the Atmosphere," *Journal of Aircraft*, Vol. 23, 1986, pp. 566-573.

[14] Atias, M. and Weihs, D., "Motion of Aircraft Trailing Vortices Near the Ground," *Journal of Aircraft*, Vol. 21, 1984, pp. 783-786.

[15] Schiling, V. K., "Motion and Decay of Trailing Vortices Within the Atmospheric Surface Layer," *Beitr. Phys. Atmos.*, Vol. 65, 1992, pp. 157-169.

[16] Corjon, A., Risso, F., Stoessel, A., and Poinsot, T., "Three-Dimensional Direct Numerical Simulations of Wake Vortices: Atmospheric Turbulence Effects and Rebound with Crosswind," *78th AGARD-FDP Symposium on The Characterization and Modification of Wakes from Lifting Vehicles in Fluids*, Trondheim, Norway, May 1996.

[17] Proctor, F. H., Hinton, D. A., Han, J., Schowalter, D. G., and Lin, Y. -L., "Two-Dimensional Wake Vortex Simulations in the Atmosphere: Preliminary Sensitivity Studies," *35th Aerospace Sciences Meeting & Exhibit*, Reno, NV, AIAA Paper No. 97-0056, January 1997.

[18] Schowalter, D. G., DeCroix, D. S., Switzer, G. F., Lin, Y. -L., and Arya, S. P., "Toward Three-Dimensional Modeling of a Wake Vortex Pair in the Turbulent Boundary Layer," *35th Aerospace Sciences Meeting & Exhibit*, Reno, NV, AIAA Paper No. 97-0058, January 1997.

[19] Han, J., Lin, Y. -L., Schowalter, D. G., Arya, S. P., and Proctor, F. H., "Large-Eddy Simulation of Aircraft Wake Vortices: Atmospheric Turbulence Effects," *12th Symposium on Boundary Layers and Turbulence*, Vancouver, Canada, July-August 1997, pp. 237-238.

[20] Han, J., Lin, Y. -L., Arya, S. P., and Kao, C., "Large-Eddy Simulation of Aircraft Wake Vortices: Atmospheric Turbulence Effects," *NASA First Wake Vortex Dynamic Spacing Workshop*, Proceedings, Hampton, VA, NASA CP-97-206235, May 1997, pp. 131-144.

[21] Darracq D., Corjon, A., Ducros F., Keane M. and Buckton D., "Three-dimensional Numerical Simulation of Wake Vortex Detection with the MELAME 2 micron Lidar." *36th Aerospace Sciences Meeting & Exhibit*, Reno, NV, AIAA Paper No. 98-0666, January 1998.

[22] Proctor, F. H., "The Terminal Area Simulations System, Volume 1: Theoretical Formulation," NASA Contrator Report 4046, DOT/FAA/PM-86/50, April 1987. [Available from NTIS]

[23] Schowalter, D. G., DeCroix, D. S., Proctor, F. H., Lin, Y.-L., Arya, S. P., and Kaplan, M. L., "Turbulent Statistics in the Atmospheric Boundary Layer: A Comparison of Large Eddy Simulation with Observations," *11th Symposium on Boundary Layers and Turbulence*, Charlotte, NC, March 1995, pp. 552-555.

[24] Bradshaw, P., "The Analogy between Streamline Curvature and Boyancy in Turbulent Shear Flows," *Journal of Fluid Mechanics*, Vol. 36, 1969, pp. 177-191.

[25] Proctor, F.H., "'A LES Subgrid Turbulence Model with Rotational Dampening," *to be submitted as a NASA Tech Report*, 1999.

[26] Han, J., "Large Eddy Simulations of Aircraft Wake Vortices In a Homogeneous Atmospheric Turbulence,", Ph. D. Dissertation.

North Carolina State University.

[27] Arakawa, A., "Computational design for long-term numerical integration of the equations of fluid motion: Two-Dimensional Incompressible Flow, Part I., *J. Comp. Phys.*, Vol. 1, 1966, pp. 119-143.

[28] Proctor, F. H., "The NASA-Langley Wake Vortex Modeling Effort in Support of an Operational Aircraft Spacing System," *36th Aerospace Sciences Meeting & Exhibit*, Reno, NV, AIAA Paper No. 98-0589, January 1998.

[29] Heinrichs, R. Rm., Dasey, T.J., Matthews, M.P, Campbell, S. D., Freehart, R. E., Perras, G. H., and Salamitou, P., " Measurements of Aircraft Wake Vortices at Memphis International Airport with a CW CO_2 Coherent Laser Radar," *Proc. SPIE 10th International Aerosense Symposium, Air Traffic Control Technologies II*, Vol. 2737, , 1996, pp. 122-133.

[30] Matthews, M., Dasey, T.J., Perras, G. H., and Campbell, S. D., " Planetary Boundary layer Measurements for the Understanding of Aircraft Wake Vortex Behavior," *Pro. Seventh AMS Conference on Aviation Weather Systems*, Feb. 2-7, 1997, Long Beach, CA.

[31] Sarpkaya, T., "Decay of Wake Vortices of Large Aircraft," *AIAA Journal*, Vol. 36, 1998, pp. 1671-1679.

[32] Campbell, S. D., Dasey, T. J., Freehart, R. E., Heinrichs, R. M., Matthews, M. P., Perras, G. H., and Rowe, G. S., "Wake Vortex Field Measurement Program at Memphis, TN Data Guide," *Project Report: NASA/L-2*, January 1997. [Available from NTIS]